Collaborative R&D with First Solar on Understanding Performance Limitations in CdTe (Project 1 “CdTe” - Mods 0-10, 13, 14-A1, 17)

Cooperative Research and Development Final Report

CRADA Number: CRD-13-00507

NREL Technical Contact: Craig Perkins

NREL is a national laboratory of the U.S. Department of Energy
Office of Energy Efficiency & Renewable Energy
Operated by the Alliance for Sustainable Energy, LLC

This report is available at no cost from the National Renewable Energy Laboratory (NREL) at www.nrel.gov/publications.

Contract No. DE-AC36-08GO28308

Technical Report
NREL/TP-5K00-87513
September 2023

Collaborative R&D with First Solar on Understanding Performance Limitations in CdTe (Project 1 "CdTe" - Mods 0-10, 13, 14-A1, 17)

Cooperative Research and Development Final Report

CRADA Number: CRD-13-00507

NREL Technical Contact: Craig Perkins

Suggested Citation
Perkins, Craig. 2023. *Collaborative R&D with First Solar on Understanding Performance Limitations in CdTe (Project 1 "CdTe" - Mods 0-10, 13, 14-A1, 17): Cooperative Research and Development Final Report, CRADA Number CRD-13-00507.* Golden, CO: National Renewable Energy Laboratory. NREL/TP-5K00-87513.
https://www.nrel.gov/docs/fy23osti/87513.pdf.

NREL is a national laboratory of the U.S. Department of Energy
Office of Energy Efficiency & Renewable Energy
Operated by the Alliance for Sustainable Energy, LLC

This report is available at no cost from the National Renewable Energy Laboratory (NREL) at www.nrel.gov/publications.

Contract No. DE-AC36-08GO28308

Technical Report
NREL/TP-5K00-87513
September 2023

National Renewable Energy Laboratory
15013 Denver West Parkway
Golden, CO 80401
303-275-3000 • www.nrel.gov

NOTICE

This work was authored by the National Renewable Energy Laboratory, operated by Alliance for Sustainable Energy, LLC, for the U.S. Department of Energy (DOE) under Contract No. DE-AC36-08GO28308. Funding provided by U.S. Department of Energy Office of Energy Efficiency and Renewable Energy Solar Energy Technologies Office. The views expressed herein do not necessarily represent the views of the DOE or the U.S. Government.

Cover Photos by Dennis Schroeder: (clockwise, left to right) NREL 51934, NREL 45897, NREL 42160, NREL 45891, NREL 48097, NREL 46526.

Cooperative Research and Development Final Report

Report Date: September 13, 2023

In accordance with requirements set forth in the terms of the CRADA agreement, this document is the CRADA final report, including a list of subject inventions, to be forwarded to the DOE Office of Scientific and Technical Information as part of the commitment to the public to demonstrate results of federally funded research.

Parties to the Agreement: First Solar, Inc.

CRADA Number: CRD-13-00507

CRADA Title: Collaborative R&D with First Solar on Understanding Performance Limitations in CdTe (Project 1 "CdTe" - Mods 0-10,13,14-A1,17)

Responsible Technical Contact at Alliance/National Renewable Energy Laboratory (NREL):

Craig Perkins | craig.perkins@nrel.gov (for Wyatt Metzger and Rommel Noufi)

Name and Email Address of POC at Company:

Rouin Farshchi, Rouin.Farshchi@firstsolar.com (for Markus Gloeckler | mgloeckler@firstsolar.com)

Sponsoring DOE Program Office(s):

Office of Energy Efficiency and Renewable Energy (EERE), Solar Energy Technologies Office

Joint Work Statement Funding Table showing DOE commitment:

Estimated Costs	NREL Shared Resources a/k/a Government In-Kind
Original Agreement, Mod 0	$40,000.00
Modification #1	$892,013.00
Modifications #2 - 10	$0.00
Modification #13	$0.00
Modification #14-A1	$.00
Modification #17	$.00
TOTALS	$932,013.00

Executive Summary of CRADA Work:

Note: Minor adjustments were made to the following original abstract as the work progressed over many years of agreement modifications/extensions; however, this version generally represents the work done.

This CRADA involves analyses on a variety of CdTe and CdTe-PV related materials, test structures, and solar cells produced at FSLR or NREL. Single-crystal (sx) material will be primarily MBE grown and provided by FSLR. Joint activities are focused on establishing the appropriate quality metrics as a basis for high performing sx devices and to study the dopability of the material. Polycrystalline (px) materials will be provided by NREL, FSLR, or fabricated jointly. Px activities are focused on the characterization of performance limiting mechanisms including bulk defects, grain boundaries, and the hetero-interface. A combination of growth, characterization, and theory will be applied. Analysis will include techniques that are well established in CdTe research at NREL (e.g., LIV/DIV/CV, AS/DLTS, LTPL, TRPL) as well as techniques that have not been widely applied to the PV part of CdTe technology (e.g., PCD, CL, µPL, SE).

Summary of Research Results:

Introduction

Many priorities of the task work were changed over the long duration of this project according to how the work was progressing. There were primarily six tasks over the course of the project work, applied to slightly differing subsets of synthesis, analysis, and characterization activities. The original purpose, overview and tasks are listed and generalized here, instead of detailing an exhaustive listing of various subtle, yet specific, experimental substitutions and variations. The outcomes of the work on these six tasks are summarized below as a representative example of the most important aspects of the body of work.

An agreement modification overview is provided here for clarity:

Original Agreement (Modification 0)

Again, the original purpose, overview and tasks are listed for the six task result explanations below in lieu of detailing an exhaustive listing of various subtle specific experimental substitutions and variations.

Modifications 1, 4, 5, 7, 10, 14-A1

Although, many subtle experimental substitutions and variations were outlined in these agreement modifications over the long duration of this project, they are not all listed here as the many priorities of the task work were changed according to how the work was progressing. The most comprehensive and straightforward manner of describing the work entails the following explanation of the six tasks as a representative summation of the most important aspects of the entirety of the work.

Modification 2: Added Task 6, and Ceased Tasks 2, 3 and 5

"First Solar industrial interests and new awards will require adjustments to the work performed under the original Appendix A to CRADA # CRD-13-507. In the future, work on ***tasks 2, 3, and 5 shall cease****, work on* ***tasks 1 and 4 shall continue****, and work on* ***task 6*** *described in the paragraph below shall be added."*

Modifications 3, 6, 8, 9, 13, and 17: No added tasks.

No-cost time extension (NCTE), modified time Period Of Performance (POP), and/or modified funding without change of scope.

Modifications 11, 12, 14-A2, 15, 16 and 18, 20+: do not apply to this project documentation

Modification 19+

Modification 19, along with related additional modifications, is ongoing work related to the completed Project 1 taskwork outlined above, is intended to be documented in a separate "Project 5" final report upon completion at a later publishing date.

List of Acronyms

AS	Admittance Spectroscopy	pX	Polycrystalline material
CL	Cathodoluminescence	SE	Spectroscopic Ellipsometry
CV	Capacitance Voltage	sX	Single-crystal material
DLTS	Deep Level Transient Spectroscopy	TBD	To Be Determined
GB	Grain Boundary	TRPL	Multiwave Time-Resolved Photoluminescence
Hall	Temperature-Dependent Hall	µPL	Spatial Mapping Micro-Photoluminescence
IPE	Inverse Photoemission	UPS	Ultraviolet Photoelectron Spectroscopy
LTPL	Low-Temperature Photoluminescence	XPS	X-Ray Photoelectron Spectroscopy
PCD	Microwave Photoconductivity Decay	Thz	Terahertz Spectroscopy
2PE	Two-photon Excitation	2PE imaging	Two-photon Excitation Spatially Resolved Time-Resolved Photoluminescence
pX	polycrystalline material	XPS	X-Ray Photoelectron Spectroscopy
JV	Current-voltage	QE	Quantum efficiency
CV	Capacitance-voltage		

Statement of Work and Task Descriptions

Purpose

Establish solid characterization methods to identify performance-limiting attributes over a range of common and uncommon CdTe device structures. Evaluate several lifetime, mobility, and trap measurements over a broad range of device structures to validate commonalities in the response as well as validity of the techniques.

CRADA Overview

This CRADA (Cooperative Research and Development Agreement) will involve analyses and inter-comparisons of CdTe-related materials and devices produced at three different locations: 1) Polycrystalline materials produced at NREL using their existing process flow, 2) Polycrystalline material produced at FSLR using their standard process flows, and 3) MBE materials produced at FSLR. Analysis will include techniques that are well established in CdTe research at NREL (e.g., LIV/DIV/CV, AS/DLTS, LTPL, TRPL) as well as techniques that have not been widely applied to the PV part of CdTe technology (e.g., PCD, CL, µPL, SE). Goals range from correlating material/design/source differences with device-performance attributes, to test advanced techniques that could offer a deeper understanding of performance limitations - regardless of material source or device design. Within this context, the Statement of Work is divided into five separate Tasks. It is expected that not all the Tasks will be operating at maximum throughput at all times, but that the workload in various task will expand and contract depending on issues such as sample availability and FSLR near-term needs. This expected shifting of workload between tasks is accounted for by applying a labor multiplier that estimates an amount of the total activities will be undertaken at any given time.

A brief task description follows: **Task 1** applies electrical characterization techniques at NREL to materials and devices from all three sources with the goal of identifying commonalities in the response as well as validating techniques. **Task 2** focuses on transferring NREL knowledge regarding CdTe substrate device, and developing and testing ancillary components (i.e., contact buffer layers) consistent with the needs of FSLR. **Task 3** focuses on establishing a higher degree of understanding with regard to the theorized and measured functionality of CdTe grain boundaries existing in FSLR polycrystalline material, but placed in a broader context of grain boundaries in both NREL polycrystalline material and engineered grain boundaries. **Task 4** analyzes FSLR materials produced by MBE to determine the degree of dopant incorporation and optimization with a view to provide a practical and theoretical foundation for future doping control in polycrystalline materials. **Task 5** provides a pathway to produce TBD reference materials for FSLR. **Task 6** Advanced analytics: implements novel characterization methods and enables extraction of fundamental parameters such as bulk, surface, and grain-boundary recombination and fundamental device limitations beyond the best practices of today.

Project Taskwork Descriptions and Results

Task 1: Electrical Characterization

General Description

Apply NREL's electrical and optoelectronic characterization facilities and expertise to the study of a range of samples produced at FS and at NREL. All studies will include discussion with NREL personnel on nature of samples and in-depth analysis of results. Samples will include a range of both single crystal and polycrystalline materials and p-n junctions. Expectation is that measurement will be made in a timely manner (cue time ~< 1wk) with a maximum throughput as specified per technique.

Objective

Evaluate comparative lifetime, mobility, and trap measurements over a broad range of device structures to validate commonalities in the response as well as validity of the techniques. Establish solid characterization methods to identify performance-limiting attributes over a range of common and uncommon CdTe device structures.

Starting Tasks

- Analysis: PCD (Carrier lifetime for comparison with TRPL). Assume 30 samples/quarter, 2 hrs/sample.
- Analysis: AS/DLTS (Low-T mobility and trap energy). Assume 15 samples/quarter, 3 hrs/sample
- Analysis: T-Hall (Support of crystalline materials). Assume 9 samples/quarter, 4 hrs/sample.
- Analysis: TRPL (Including modeled parameter extraction) of interface and bulk lifetime. Assume 30 samples per quarter, 2 hrs/sample.
- Analysis: LIV/DIV/CV. Assume 30 samples/quarter, 1 hr sample.
- Synthesis: Polycrystalline materials and devices to establish commonalities and validate techniques.
- Notes:
    - The above-mentioned items are expected to represent ~80-90% of the activities.
    - Other techniques that may be needed to expedite or complement analysis include:
    - CL. Assume 15 samples/quarter, 2 hrs/sample.
    - µPL. Assume 15 samples/quarter, 3 hrs/sample.
    - GB related characterization would be covered under Task 3.

Task 1 Results

Most of the work in this task is luminescence-related, either PL,TRPL, or CL. These analytical methods are among the few that are able to probe the details of defects and dopants that are critical to the functioning of advanced PV devices. Initial work focused on type IB dopants such silver, gold, and copper, primarily copper. Throughout the history of CdTe solar technology, Cu has been critical to attain hole concentration and to form the back contact. However, the role of type IB dopants is complex. First-principles calculations indicate that increasing Cu levels can lead to formation of CuI donors that compensate Cu_{Cd} acceptors. Lifetime is affected by Cu levels, and Cu is mobile and can segregate to grain boundaries or adjacent material layers. Cu concentration is often 10^{17}–10^{18} cm^{-3}*(per cubic meter)*, yet hole concentration is several orders of magnitude lower. Utilizing PL data, we constructed a recombination model for state-of-the-art CdTe devices and demonstrate that the same Cu_{Cd} site that increases hole density can also reduce lifetime. In one study,[1] five polycrystalline films with large grains (6–10 µm) were chosen for photoluminescence (PL) analysis, because for smaller grains inhomogeneous broadening could obscure some features in the PL spectra. The films were grown in a superstrate configuration by vapor-transport deposition, annealed in a $CdCl_2$ containing atmosphere, and doped with Cu from a wet-applied Cu source followed by a thermal bake. For polycrystalline CdTe, the resulting devices have an extremely high Voc of 890–900 mV. A reference sample without intentional Cu doping had a much lower Voc of 777 mV. The high Voc of these Cu-doped solar cells can be attributed largely to an increase in the hole concentration and long lifetimes in the CdTe absorber layer. Capacitance-voltage measurements indicate a net acceptor concentration of 1E15 cm^{-3}, which is approximately an order of magnitude greater than typical CdTe solar cells. PL and electrical measurements indicate that Cu_{Cd} sites cause this hole concentration.

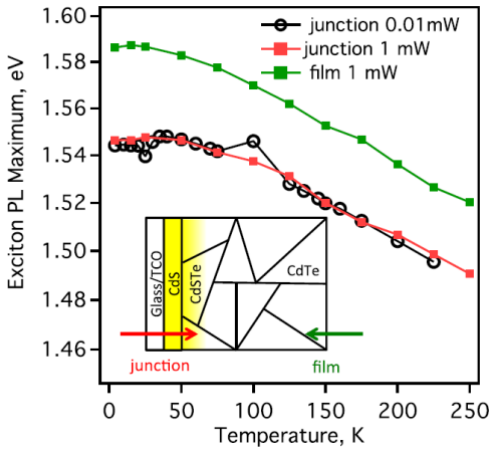

Figure Task 1.1 Exciton PL emission temperature dependence for measurements from the film (CdTe, green) and junction (CdSTe, red) sides as illustrated in the inset. When lower excitation power is used (black), the exciton PL energy is essentially identical.

Figure Task 1.1 illustrates the temperature-dependent shift of the exciton band observed at high energy in 5 K PL spectra (not shown). Data show that the device has different Eg values at the junction and back-contact regions. The difference DEg»40 meV is attributed to formation of a CdSTe alloy at the junction. Ellipsometry data indicate this energy shift corresponds to a CdS_xTe_{1-x} composition with x»0.05. The measurements described below were repeated for both sides of the photovoltaic device: the CdS/CdTe junction where CdSTe alloy properties were

evaluated, and the CdTe film side (see inset in Fig. 2). The absolute Eg values were estimated from the data in Figure Task1.1 by adding the free exciton binding energy (»10 meV) and exciton-defect binding energy (10–20 meV). From 50 to 250 K, the Eg shift is measured to be approximately 0.3 meV/K. A similar result was reported for CdTe single crystals.

In this study we examined the doner-acceptor pair (DAP) binding energy by varying the electron-hole injection level. Figure Task1.2 shows PL emission spectra from the junction side when excitation power was varied from 3 µW to 11 µW.

The dependence of the broad DAP peak on the excitation power, I_{EXC}, can be analytically described:

$$I_{EXC} = D\frac{(h\nu_{max} - h\nu_{\infty})^3}{h\nu_B + h\nu_{\infty} - 2h\nu_{max}}\exp\left(-\frac{2(h\nu_B - h\nu_{\infty})}{h\nu_{max} - h\nu_{\infty}}\right)$$

where D is a coefficient, hu_{max} is the experimental DAP energy, $hu_{¥}=E_g-E_a-E_d$ is the limiting photon energy of infinitely distant pairs, and $hu_B=E_B+ hu_{¥}$ with $E_B=e^2/4\pi\varepsilon\varepsilon_0R_B$ (R_B is Bohr radius of the shallow impurity). Data in the inset indicate $hu_{¥}=1.336$ eV. The previous equation predicts that the blue shift due to Coulombic interaction is at most the binding energy of the shallow impurity. For CdTe, shallow donors form with E_d»10 meV below the conduction band. Consistent with this estimate, when excitation power is increased by almost four orders of magnitude, the DAP band shifts by »10 meV. Fitting these data gives $hu_B=1.36$ eV and $R_B=66$Å. The large Bohr radius is consistent with the small donor ionization energy. Taken together, the data indicate $E_a+E_d=0.16$ eV, and most of this energy is attributed to E_a because E_d is small.

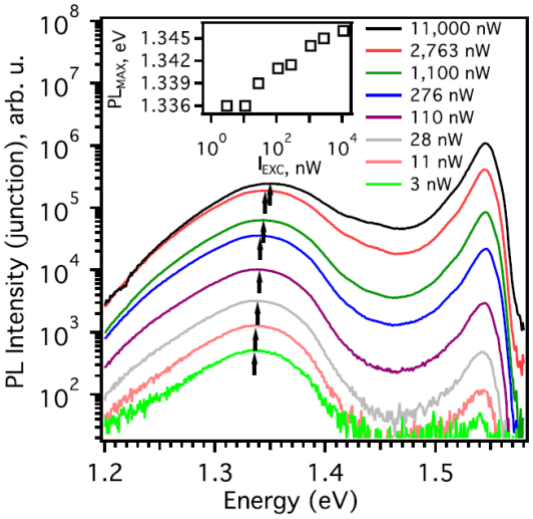

Figure Task 1.2 PL emission spectra at 5K from the junction side of the device as a function of excitation power (see legend). Arrows indicate the DAP band maxima. The inset shows the DAP PL shift with excitation power.

Figure Task1.3 shows an Arrhenius analysis of Shockley-Read-Hall (SRH) recombination at higher temperatures done by comparing TRPL lifetimes for undoped single-crystalline CdTe, a polycrystalline CdTe device without intentional Cu, and a high-voltage device with Cu-doping. For the single-crystal reference sample, the lifetime has relatively weak temperature dependence and changes from 360 to 383 ns at 275–200 K.

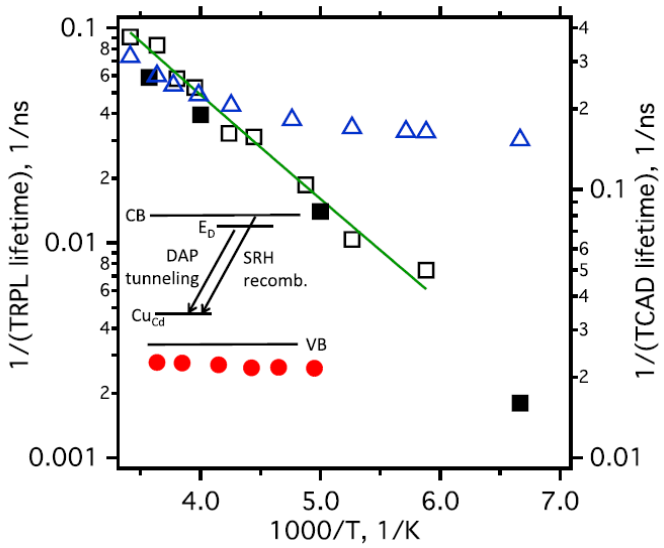

Figure Task 1.3 Recombination rates (TRPL lifetime)1, as a function of temperature for single-crystal CdTe (red circles), undoped CdS/CdTe (blue triangles), and doped CdS/CdTe (open black squares). The solid line shows an Arrhenius fit for the Cu-doped sample. Filled squares show recombination rates from TCAD simulations assuming NA=1017 cm3, ND=9 x 1016 cm3, electron capture cross-section 5 x 1015 cm2, and temperature-independent electron mobility 50 cm2/(V s). The inset shows the recombination model that includes DAP tunneling and SRH recombination.

Arrhenius-like temperature dependence for capture cross-sections has been identified for non-radiative multiphonon transitions due to deep levels in some semiconductors, such as GaAs and GaP. Because the lifetime temperature dependence is very different for the single-crystal and Cu doped/undoped polycrystalline CdTe, it does not appear that a common deep defect can explain our experimental data, unless deep levels are created by Cu.

It is plausible that the lifetime decrease from 134 ns (170 K) to 11 ns (295 K) occurs due to relatively shallow recombination centers. The PL emission data indicate the presence of acceptors »150 meV above the valence band and shallow donors. Radiative lifetime at this doping is »10 µs,44 while experimental lifetimes range from 500 to 11 ns. Therefore, SRH recombination is dominant.

The shift of the Fermi level with temperature will depend on the distribution of defects, and the PL spectra indicate the presence of both donors and acceptors. Time-resolved photoluminescence simulations were performed with code written in Sentaurus Device to analyze the role of compensation on lifetime temperature dependence. Without a large concentration of compensating donors, the Fermi level can move both above and below the E_a=150 meV defect and produce trends that are not observed here. In the case of strong compensation, the Fermi energy temperature variation is reduced, and the Cu_{Cd} recombination site can generate results consistent with the experimental data in Fig. Task1.3. Both donors and acceptors have been observed in the PL spectra here, and compensation has been widely reported in CdTe. So the PL and TRPL data can be consistently explained with the recombination model in Fig. Task1.3. At low temperatures, recombination happens by DAP tunneling. At higher temperatures, nonradiative SRH recombination from Cu_{Cd} states describes the data.

Task 2: Substrate Device Development

(Note: Task 2 work was ceased per Modification 2)

General Description

Evaluation of process and material options to identify optimal process flow for a substrate devices with acceptable back-contact quality, bulk doping, and high absorber lifetime. Data derived from FS material and interactions will be unique to FS.

Objective

Co-development of substrate-mode test structure CdTe device with a goal of exceeding 900mV Voc. Confirm device design criteria for optimal hetero-junction design on a CdTe platform.

Starting Tasks

- Synthesis/Analysis: Develop a working back contact that is robust to subsequent process steps.
- Synthesis/Analysis: Comparative study of alternative junction partners (or buffers) including but not limited to sputtered CdS, evaporated CdS, or Zn(O,S).
- Synthesis: Absorber layers may be deposited and annealed at FSLR or NREL
- Synthesis: Window layers may be deposited at FSLR or NREL.
- Synthesis: Validation of a sputtering approach for substrate devices, by paralleling for select material systems a deposition/characterization flow w/o vacuum break.
- Analysis: Characterization of the band-offset by XPS/UPS/IPE on select devices in substrate configuration.

Task 2 Results

Substrate-oriented CdTe was considered as a clean test bed for front buffer studies. NREL fabricated cells using their previously designed structure (Figure Task 2.1) to typical efficiencies of ~10% (Figure Task 2.2), with open-circuit voltage (Voc) values capable of exceeding 800 mV.

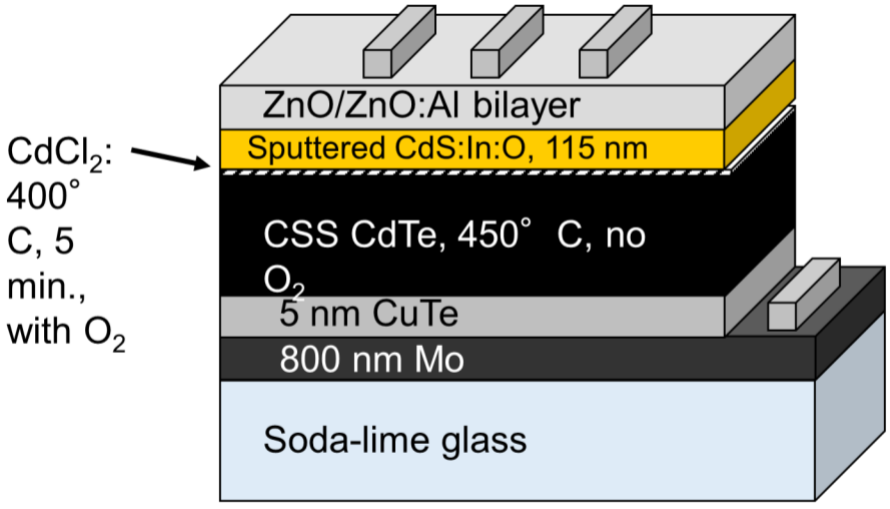

Figure Task 2.1 Substrate device structure

Oxygen was excluded from the close-spaced sublimation (CSS) CdTe deposition ambient but incorporated in the CSS vapor $CdCl_2$ heat treatment ambient and the sputtered CdS:In ambient. A thermal anneal at 250 °C was performed after deposition of the ZnO/ZnO:Al bilayer. This step had proven critical in previous work, improving all device parameters; efficiency typically improved by several absolute percent as a result. This anneal may have led to mitigation of interfacial defects at the main junction. Significant rollover was observed in current density-voltage (JV) curves, as was typical for this structure because of back contact limitations.

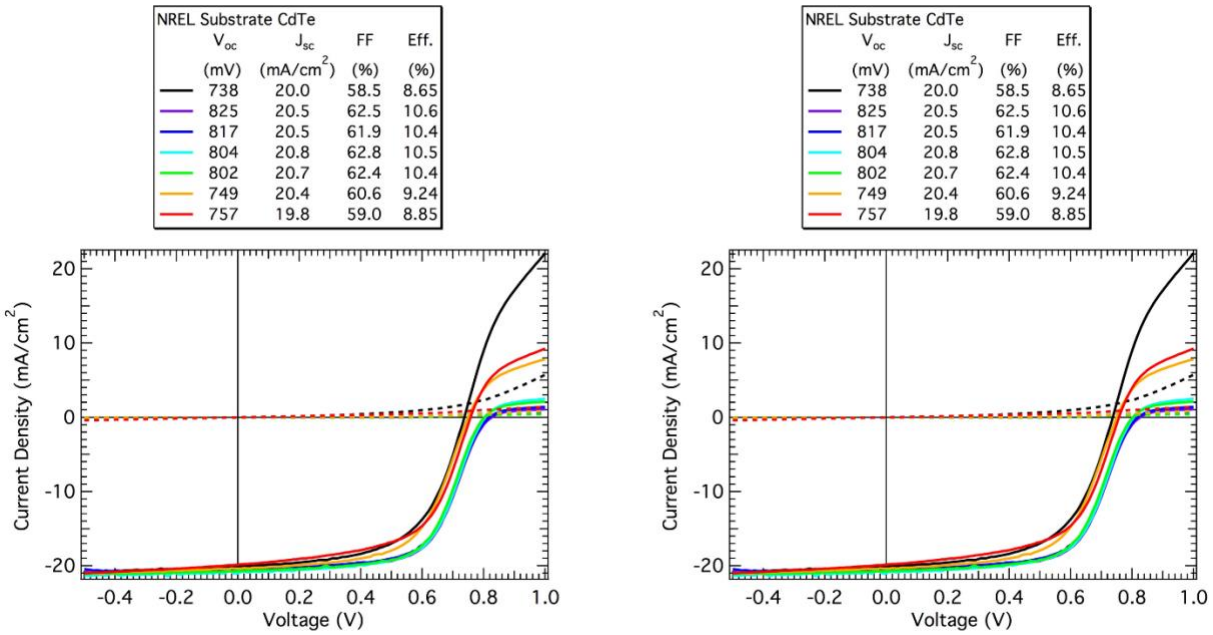

Figure Task 2.2. Best substrate devices are above 10%

Substituting CdS provided by First Solar resulted in much lower initial JV performance (Figure Task 2.3), due to lower values for all JV parameters. Though the 250 °C anneal was performed after the CdS deposition rather than after deposition of the ZnO/ZnO:Al bilayer, this was not expected to be detrimental based on previous work. The origin of the lower performance was not determined. Because First Solar implemented a CdTe single-crystal device test bed independently and chose to use this for future front buffer studies, the substrate-oriented CdTe work was not pursued further.

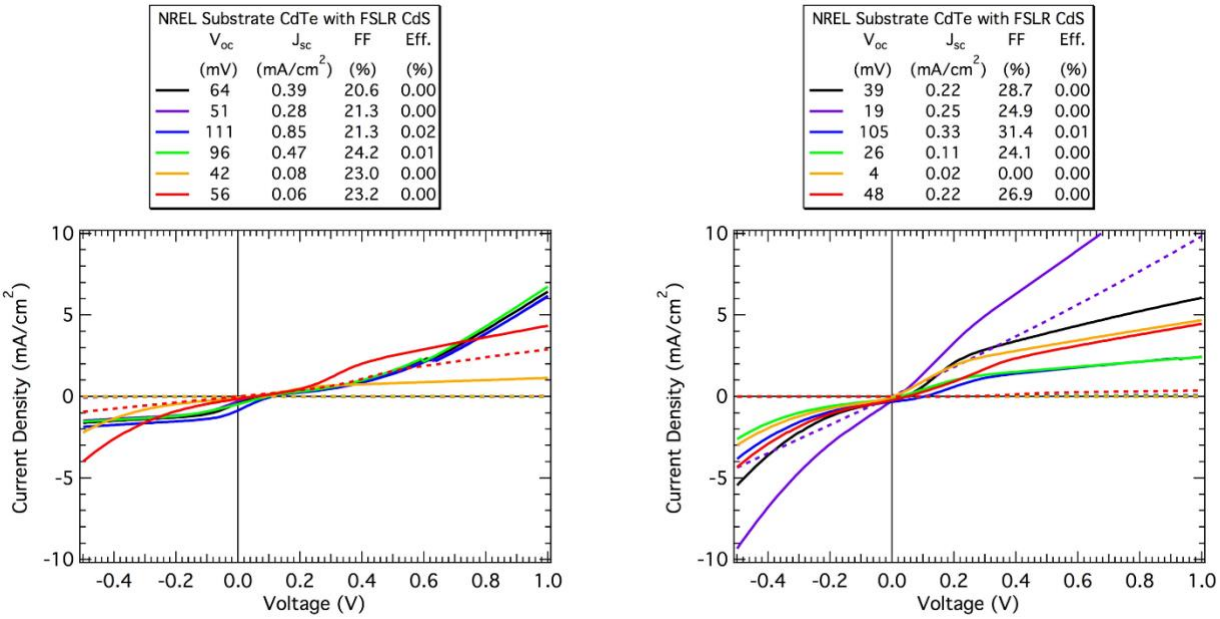

Figure Task 2.3. Substrate devices using First Solar-grown CdS emitters

Task 3: Fundamental GB Studies

(Note: Task 3 work was ceased per Modification 2)

General Description

Utilize process flows at FSLR and NREL to build a variety of GB structures using px or sx materials. Characterization techniques currently available or under development at NREL will be utilized to study the electronic nature of GBs. First principle calculation will be used to explore plausible models for GBs structure (extended defect formation and activation energy, potential passivation strategies). Data derived from FS material and interactions will be unique to FS.

Objective

The electrical properties (extended defect characteristics, origin, density) of GBs in CdTe will be studied over a range of process and performance windows. These results will enhance understanding of GB properties to device performance.

Starting Tasks

- Theoretical: Model band structure and electrical activity (traps) of various GB types to identify worst actors from first principle.
- Theoretical: Model changes to GB properties by passivation with impurities.
- Synthesis: Create samples with variety of typical GBs, engineered GBs, and GB that incorporate various passivation/impurity chemistries. Samples (sx and px) preparation expected at both NREL and FSLR.
- Analysis: Micro-analytical characterization of dominant defects at GBs w.r.t. misorientation & twins for a variety of samples from different process conditions and passivation techniques using tools such as EBSD, CL, and µPL.
- Analysis: Macro-analytical characterization to validate or improve first principle models using tools such as PL and AS/DLTS. Correlate observed defects to specific or predicted GB configurations.

Task 3 Results

Although Task 3 was discontinued early in this project, work done to study fundamental properties of grain boundaries was important in follow-on studies and in fact grain boundary work continues to this today folded into other tasks. This section has an overview of grain boundary studies that were done during the time Task 3 was active.

Grain boundaries in polycrystalline materials have profound effects on the intrinsic defects as well as the incorporation of extrinsic defects such as dopants. The reverse is true as well: extrinsic defects can affect grain boundaries. As an example of the latter, Figure Task 3.1 shows an early EBSD micrograph of a “run away” doping operating involving arsenic. During MBE growths of CdTe:As, at certain high fluxes of arsenic dopant (cadmium arsenide, Cd_3As_2), the enough defects form such that the crystallographic order of the underlying CdTe substrate is lost and the growth surface devolves into fine-grained polycrystalline material that is largely Cd_3As_2 rather than the desired doped CdTe:As. Thus one of the early lessons learned was upper bounds for dopant fluxes and arsenic incorporation.

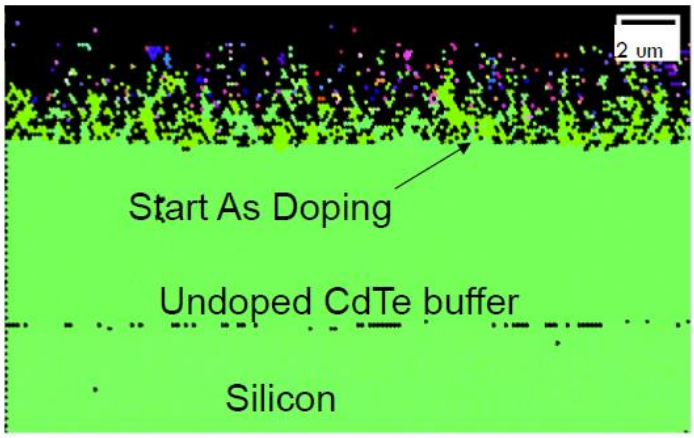

EBSD cross section of epitaxial layers

Figure Task 3.1. Cross sectional EBSD showing loss of crystallinity during arsenic doping.

A broad overview of some of these early grain boundary studies is shown in Figure Task 3.2. Here one can see that longest typical carrier lifetimes show correlation with grain size, indicating that recombination at grain boundaries is high. Extrinsic Group V doping was also limited in the smallest grained material, showing the importance of different chemical environments at the grain boundaries versus the grain interiors.

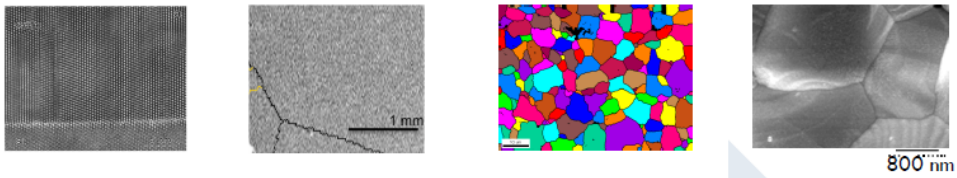

sX layer	Bicrystals/ mm grains	10 - 100 µm grains	Standard material
Holes (cm^{-3})	> 10^{16} cm^{-3}	> 10^{16} cm^{-3}	> 10^{16} cm^{-3}	> 10^{15} cm^{-3}
Lifetime (ns)	5 – 400 ns	5 – 40 ns	0.5 – 40 ns	1- 5 ns
Interface (cm/s)	250 – 50000	10^4 – 10^6	10^4 – 10^6	10^4 – 10^6
Back contact	FF 40 - 65 %	NA	NA	NA
Transmission	Not optimized	Not optimized	Not optimized	Not optimized

Figure Task 3.2. Table of electro-optical properties of CdTe materials for materials varying in grain boundary volume.

Task 4: Extrinsic Doping Studies

General Description

Focus will be on sx materials and related device architectures. Dopants may be introduced by various means and annealing processes may be explored to modify dopant activation. First principle calculations will be used to validate the findings of AS and DLTS measurements. Some overlap with activities of Task 1 is expected.

Objective

Identify the electronic properties of p-type and n-type dopants in sx CdTe and related ternary alloys.

Starting sub-tasks

- Theoretical: Evaluate dopant choices and strategies by first-principle calculations for CdTe and ternary relatives.
- Synthesis: Produce samples by appropriate processes (diffusion, implantation, in-situ, etc.)
- Analysis: Characterize energy level (activation energy) of resulting samples by appropriate means (Hall, PL, AS, etc.)

Task 4 Results

Group V doping of polycrystalline CdTe based thin-films is a critical area of research for this PV technology as potential means to improve p-type carrier concentrations, lifetimes, and ultimately efficiency together with device stability over long periods of operation. In order for group V dopants (N, P, As, Sb, and Bi) to contribute to p-type acceptor densities in a CdTe based lattice, they need to sit on the anion (Te) sites. Group V dopants siting in other lattice locations may compensate the material as n-type donors, deep recombination centers, and/or neutral defects. Ideally controlling this lattice position would happen during the deposition of the material, but given the ultra-fast nature of CdTe thin-film deposition process that has enabled it to be a highly competitive PV technology, this control may be limited. As such, post deposition “activation” processes are necessary to move group V elements from various incorporated locations to anion sites. A common process in activation efforts such as this involves the use of cation (Cd) overpressure anneals. The idea here is to ensure cation sites are filled with the desired cation species (Cd) and potentially generate anion (Te) site vacancies for the anion site dopant (N, P, As, Sb, Bi) to occupy. NREL has the capability to perform such anneals, so much of the group V doping effort involved this idea/process in some way. Figure 1 shows a schematic for one implementation of an anneal process that was used for this work using a sealed ampoule in a 3-zone furnace followed by a rapid quench in a water bath.

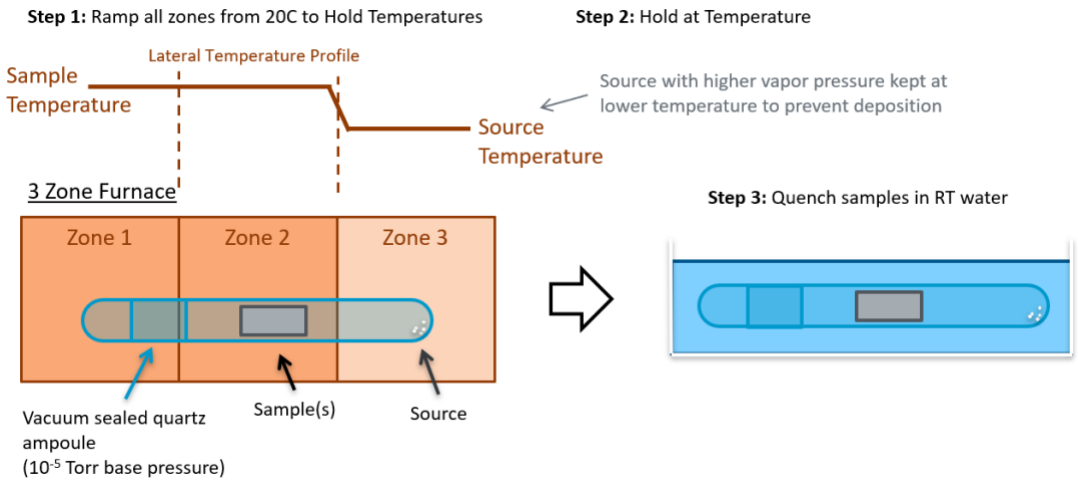

Figure Task 4.1 – Sealed ampoule anneal process.

A much more ubiquitous process in CdTe-PV device processing is a post deposition halide treatment (e.g., $CdCl_2$) which greatly enhances the thin-film optoelectronic performance. As such, group V activation processes also often involved halide treatments in some form and at some stage.

Investigations related to group V doping were performed at NREL and First Solar using materials deposited and activated at both institutions. Many details of these processes and resulting device performance is proprietary in nature, so details will be left out of this report. Some results of this work are shown and discussed below.

An example of some CV data for an experiment is shown in Figure 2. Red and Yellow data were from a process that did not activate the group V dopant as indicated by depletion widths of ~3 μm. The green data is from a process that seems to have activated the dopant at a low level (~1E15cm-3) while the blue data is for a process that was more successful in activating the group V dopant, achieving carrier concentrations approaching 1E16 cm-3.

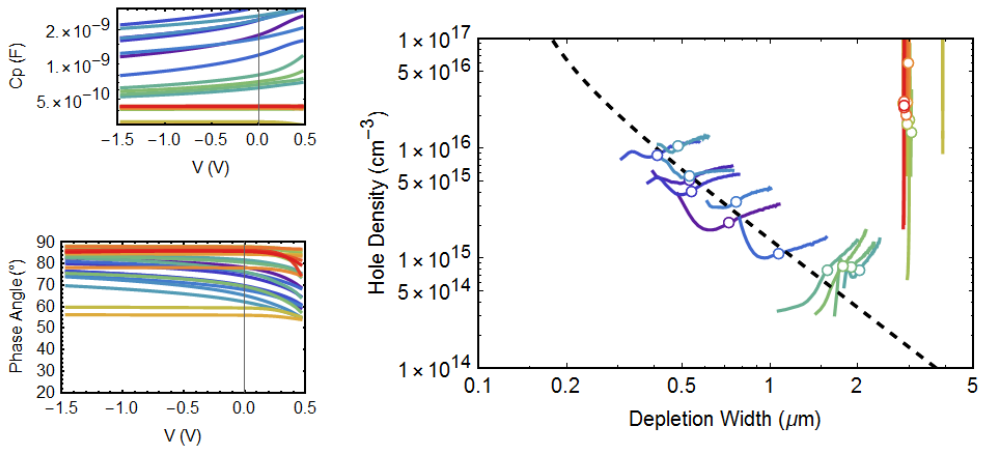

Figure Task 4.2 – CV data for an experiment.

Figure 3 shows CV results for a similar experiment in which the order of processing was found to be important for achieve good carrier concentration. The green data used process A then B and resulted in good carrier concentrations, while blue data used process B then A and resulted in poor carrier concentrations.

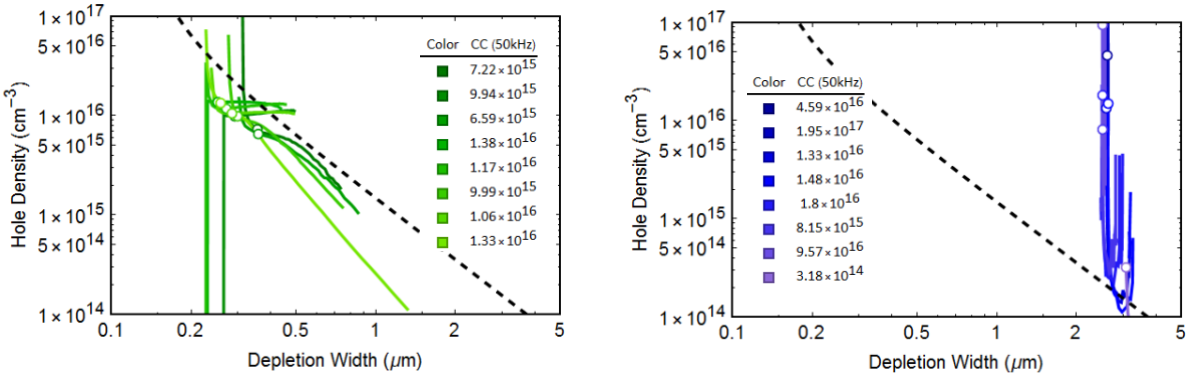

Figure Task 4.3 - CV data for an experiment.

In addition to anion site-based processes, other novel activation ideas and processes were explored. Figure 4 shows carrier concentrations extracted from CV measurements for several different processes. The 4M and EA processes are considered more typical while the A1 through A4 processes were more novel. In this case the novel treatments enabled better carrier concentrations.

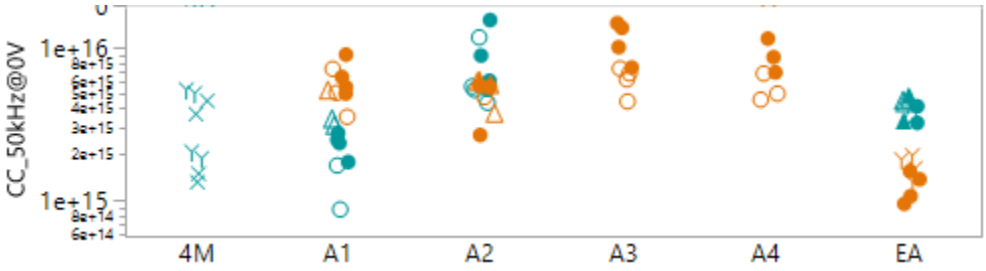

Figure Task 4.4 – Carrier concentration derived from CV measurements for devices with different processing.

Different group V dopants (N, P, As, Sb, and Bi) were explored and compared as a part of this CRADA. Figure 5 shows depletion width vs carrier concertation data extracted from CV measurements at 0V applied bias for two different group V dopants. With similar processing, similar carrier concentrations were achieved, but the associated depletion widths were different. This type of effect may have a variety of causes, but one possibility is additional charge or the presence of an undesirable dipole within the device stack that alters the CV measurement.

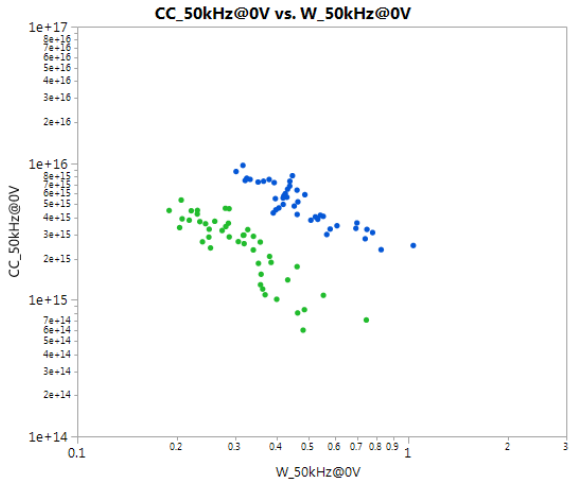

Figure Task 4.5 – 0V bias CV data for devices using two different group V dopants (blue vs green points), but otherwise receiving similar processing.

Additional characterization was also carried out on certain films at different times. Carrier lifetime is of great importance regarding the ability to achieve higher PV performance as carrier concentrations in the absorber are improved. TRPL is a common technique for measuring carrier lifetimes in semiconductor materials and was used throughout the CRADA. Figure 6 shows TRPL data for a series of samples in which a treatment was varied from a higher level to a lower level; red to blue respectively. The first part of the decay curve varied inversely with this treatment level while the "tail" of the decay seemed to improve with the level of the treatment. This is likely a result of the nature of the defects within the material following different levels of processing.

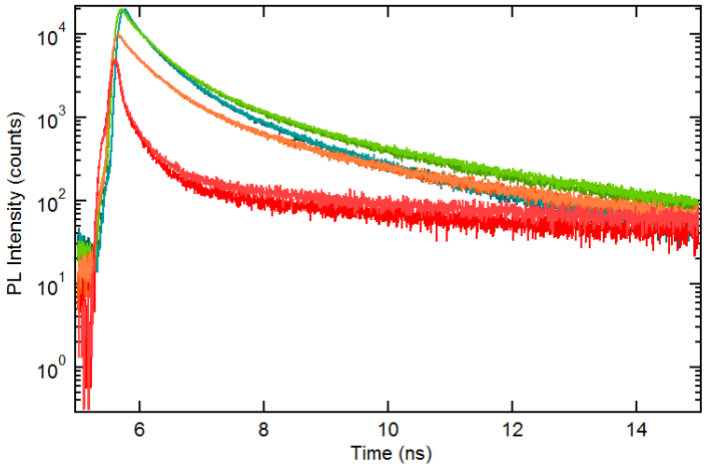

Figure Task 4.6 – TRPL data for samples that received different levels of treatment resulting in different decay profiles.

Point type defects in semiconductors play an important role in their optoelectronic performance, but so do larger extended defects, such as grain boundaries. Given this interrelationship we also analyzed these larger features is various ways. Figure 7 shows optical images of grain structure resulting from different processing and the average along with grain size statistics from those images. In this case, drastic differences in grain size were achieved with different processing which may contribute to carrier lifetimes.

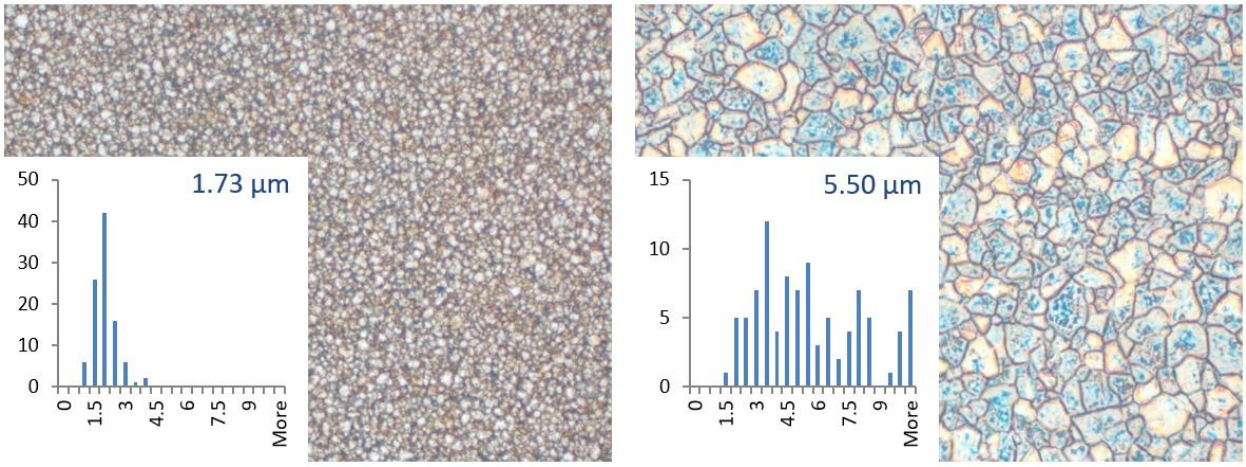

Figure Task 4.7 – Optical images and grain size statistics for 2 different post deposition processes (left vs right).

No-uniform defect distributions in px material can also affect performance. As an example, Cl at grain boundaries is considered to be primarily useful as a means to passivated more detrimental defects such as dangling bonds. Other types of accumulation may be detrimental to performance. Figure 8 shows TOF-SIMS data for a film that received a halide treatment and clearly shows the accumulation of Cl at grain boundaries. In contrast the group V dopant map shows little to no structure (grain boundary accumulation) indicating that it is distributed uniformly throughout the film.

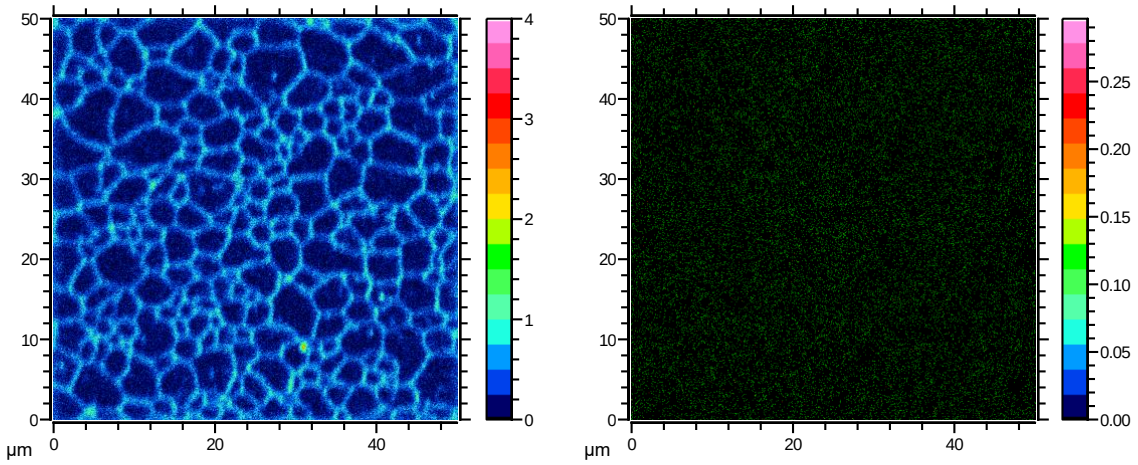

Figure Task 4.8 – TOF-SIMS analysis of a group V doped film. Left is the Cl map; Right group V dopant map.

Task 5: Reference Sample Preparation

(Note: Task 5 work was ceased per Mod 2 because of a change in priorities)

General Description

Generate NREL materials and device samples for use by FS as "reference" material utilizing existing and/or TBD process flows.

Expected Resource Requirements

- Approximately 5 samples / month

Task 5 Results

Although Task 5 was discontinued early in this project, preparation of reference samples mainly with First Solar and NREL molecular- beam epitaxy (MBE) machines was instrumental in making progress in other tasks. The grain boundary work in Task 3 for example used some single crystal films grown by MBE. MBE growth systems were used unconventionally in some cases to control purity levels in polycrystalline films. Figure Task 5.1 shows a photo of the NREL MBE machine that was brought up and running for this CRADA. The system has a base pressure of 6 x 10-10 torr, obtains a thickness uniformity of <5% across a 3" wafer, has a substrate temperature uniformity of <3% across a 3" silicon wafer, can do 1 μm/hr CdTe growth rates, and has sources for CdTe, Cd, Te, Zn, and Mg. Dopant sources are In, As, and N. In-situ characterization methods include RHEED and BandiT, the latter being used for temperature, thickness, and roughness measurement.

Figure Task 5.2a shows a photo of a high quality CdTe/Si epitaxial film, along with an X-ray diffraction rocking curve with a full width at half maximum of only 108 arc-seconds (Fig Task 5.2b). The RHEED pattern of this film in Figure Task 5.2c shows streaks rather than spots, indicative of layer-by-layer epitaxial growth.

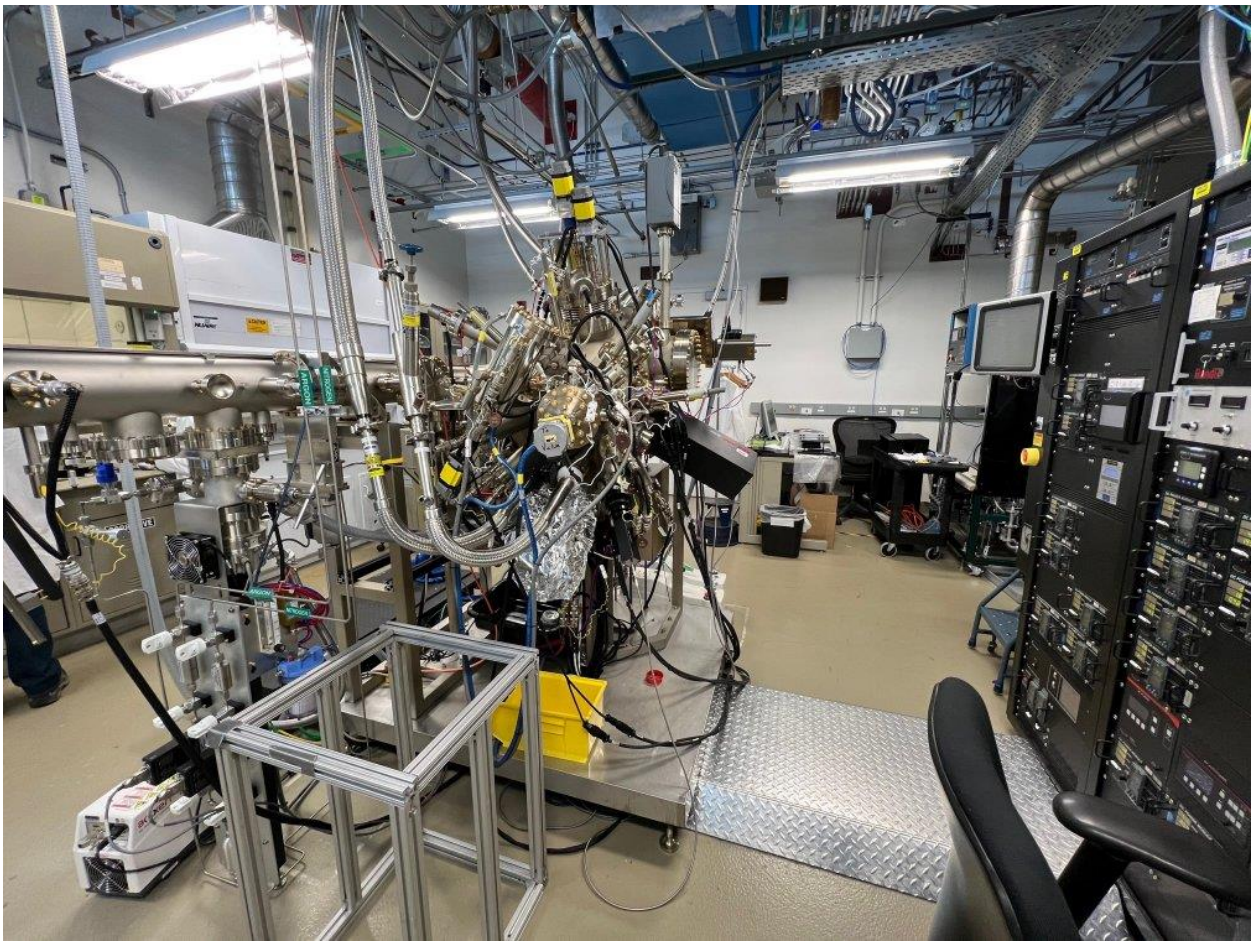

Figure Task 5.1 Photo of the NREL CdTe MBE system

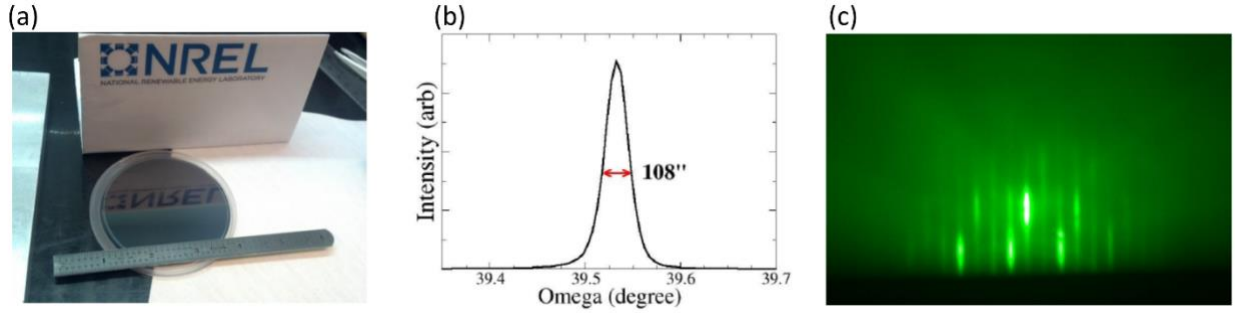

Figure Task 5.2: In (a), photo of CdTe/Si epitaxial heterostructure. In (b), X-ray rocking curve of a typical high quality film, and in (c) a RHEED pattern from same film.

Figure Task 5.3 has a summary of crystal quality as measured by X-ray rocking curves from the first 33 growth runs from the NREL MBE system. The data show problems encountered when making thin films, such as, films without an arsenic buffer layer first deposited on the silicon, when the substrate temperature was too low (i.e., polycrystalline or high fraction of amorphous material), and with run-away growths resulting from too much arsenic.

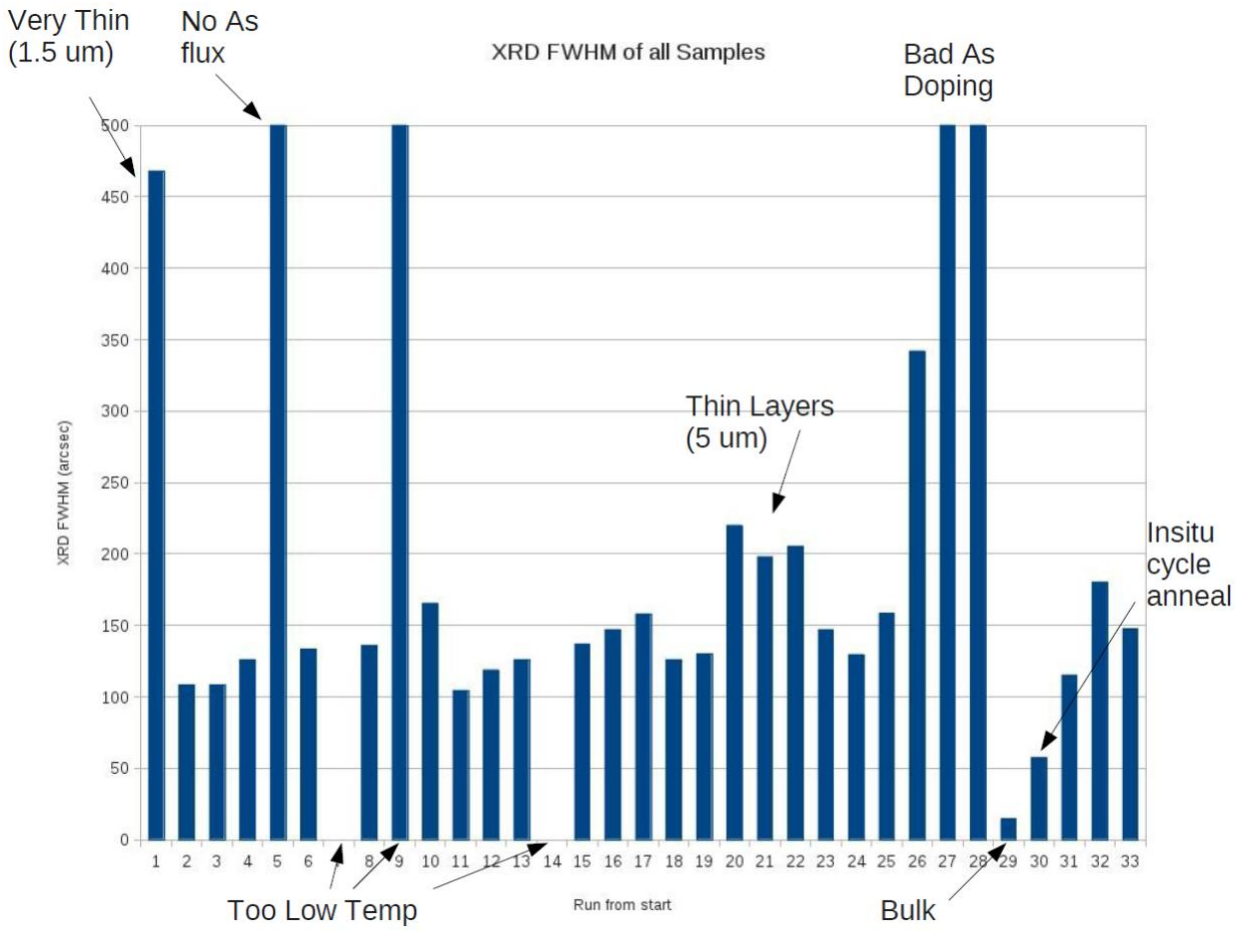

Figure Task 5.3 FWHM of X-ray rocking curves for the first 33 MBE growth runs, CdTe/Si heterostructures.

Task 6: Advanced analytics: implements novel characterization methods and enables extraction of fundamental parameters such as bulk, surface, and grain-boundary recombination and fundamental device limitations beyond the best practices of today.

General description

NREL will implement novel characterization methods and analysis together with sample sets designed from First Solar to answer fundamental questions and advance CdTe metrology.

Objective

Enable extraction of fundamental parameters such as bulk, surface, and grain-boundary recombination and fundamental device limitations beyond the best practices of today.

Task 6 Results

A lot, if not the majority, of work within this project can be binned into Task 6, "Advanced Analytics". Analytical measurements performed at NREL are listed in the Table of Acronyms earlier in this document. With a gradual change from copper to Group V doping, there has been a need for renewed examination of many aspects of cell design. One example of advanced analytics is in PL-based recombination analysis in CdTe:Cu solar cells.[2] Recombination limits open-circuit voltage (*V*OC), and many experimental techniques are used to characterize recombination with the objective to increase *V*OC in photovoltaic (PV) solar cells. Detailed models to study recombination from photoluminescence (PL) data were developed in semiconductor spectroscopy—for example in single-crystal CdTe and CdZnTe. However, PV devices are substantially different from single crystal semiconductors. Thin-film PV devices typically employ polycrystalline semiconductors, include p-n junctions in the semiconductor region of interest, and sometimes include compositional variations from the parent semiconductor structure (such as CdTe alloying with S in the p-n junction region of CdS/CdTe solar cells). Most PL-based studies were applied to polycrystalline films—not PV devices. NREL and First Solar have worked together to take PL-based analysis of solar cells to new levels of sophistication. Figure Task 6.1 shows an example of this in which PL was used on high voltage devices rather than simple film stacks, and in which sophisticated modeling was done to better understand the results.[2] A clear correlation between device Voc and minority carrier lifetime is seen in Figure Task 6.1. The good agreement between experimental data and TCAD simulation results suggests that device physics is accurately described by the model used.

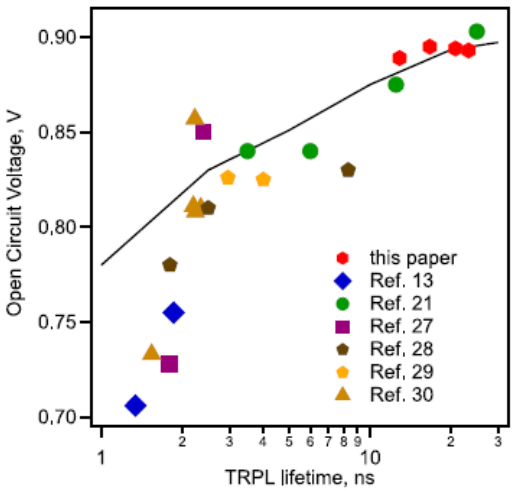

Figure Task 6.1 Device Voc versus TRPL-measured lifetimes. Solid line is simulation.

Another type of luminescence, cathodoluminescence done in a modified scanning electron microscope, was also used to study band tails and spatial fluctuations in electronic properties in CdTe and CdSeTe materials and devices. Fluctuations refer to inhomogeneity in the distribution of donors and acceptors at the nanometer scale and occur in many compound solar cell materials such as $Cu(In,Ga)Se_2$, $Cu_2ZnSn(S,Se)_4$, and $CdSe_xTe_{1-x}$. In this work,[3] numerical simulations show that these fluctuations produce not only electrostatic potential variation, but also, local changes in the carrier density and effective bandgap. For a $CdSe_xTe_{1-x}$ absorber doped with arsenic, simulations and cathodoluminescence data within single grains demonstrate how donor and acceptor densities—consistent with capacitance-voltage and secondary-ion mass-spectrometry data—produce tails in photoluminescence, quantum efficiency, and absorption measurements. In Figure Task 6.2 we compare CL spectra for $CdSe_xTe_{1-x}$:Cu and $CdSe_xTe_{1-x}$:As devices, which have representative FWHM values for their respective peak energies (1.40–1.43 eV). These spectra show that, for equal peak energies, the low-energy tail is generally wider for alloyed materials doped with arsenic than with copper. Moreover, if the CL peak energy is primarily a function of the local alloy composition, then arsenic doping consistently enhances the tail width relative to copper doping for $CdSe_xTe_{1-x}$ alloys of various compositions.

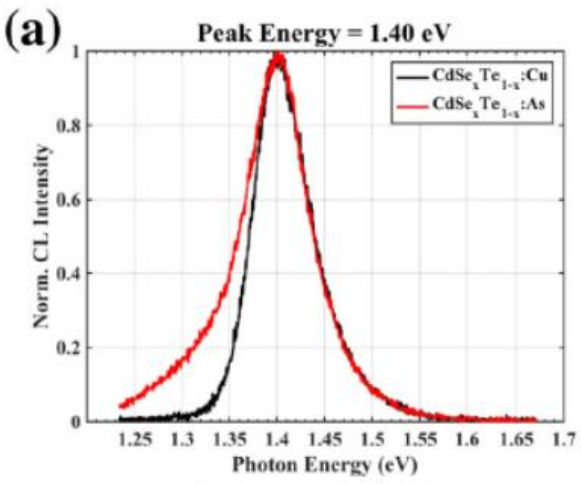

Figure Task 6.2 CL spectra comparing copper and arsenic dopants

Figure Task 6.3 visualizes potential fluctuations created by randomly distributed donors and acceptors. We distributed donors and acceptors in a 250 × 250 × 250 nm^3 cube volume using a random number generator to determine the *x*, *y*, and *z* coordinates of each defect. In (a) we plot 703 donors and 859 acceptors, corresponding to p_{avg}=10^{16} cm^{-3} and $N_{t,avg}$=10^{17} cm^{-3}, for 10% dopant activation. We let each defect contribute a screened Coulomb potential to the potential distribution and the overall potential at each point in the cube is given by the sum of potentials from all defects. In (b) is shown the potential distribution in the plane defined by *z*=125 nm for p_{avg}=10^{16} cm^{-3}, $N_{t,avg}$=10^{18}cm^{-3}, and 1% dopant activation. The fluctuations are clear.

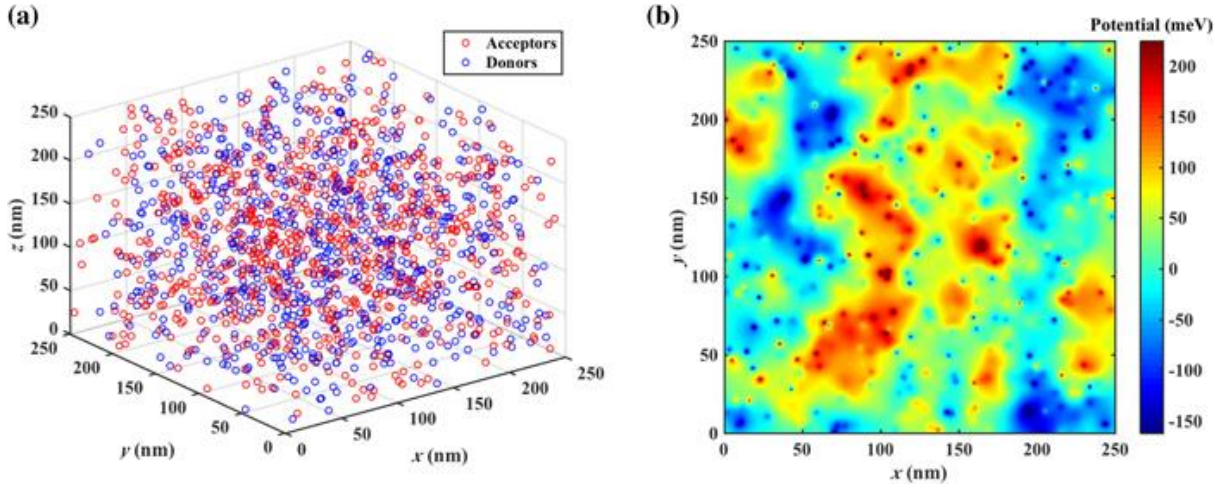

Figure Task 6.3(a) Randomly distributed donor and acceptor defects in a 250 × 250 × 250 nm3 cube. In (b) is shown the potential distribution in the plane defined by z=125 nm

Another type of advanced characterization conducted in Task 6 was focused on interfacial properties. In Figure Task 6.4 is shown XPS results for Group V-doped devices that were thermomechanically separated at the oxide-absorber interface. Panel (a) shows high resolution core level data from the arsenic 2p$_{3/2}$ region taken from arsenic doped samples while panel (b) shows data from the Sb 3d$_{3/2}$ region for antimony doped films. Notable in these spectra are that dopants are segregated to very high concentrations in a thin layer on the oxide side of the interface only, ~1000 times higher than in the bulk of the films. Comparison of the peak

positions for both arsenic and antimony indicate that the dopants are in the cationic form rather than the electrically active and desired anionic form. One important conclusion from this work[4] is that catalytic oxidation of dopants caused by the TCO cause segregation of Group V dopants and thus de-doping of some parts of the device stack under certain conditions. Tuning of processing conditions to allow activation and avoid this segregations is an ongoing work.

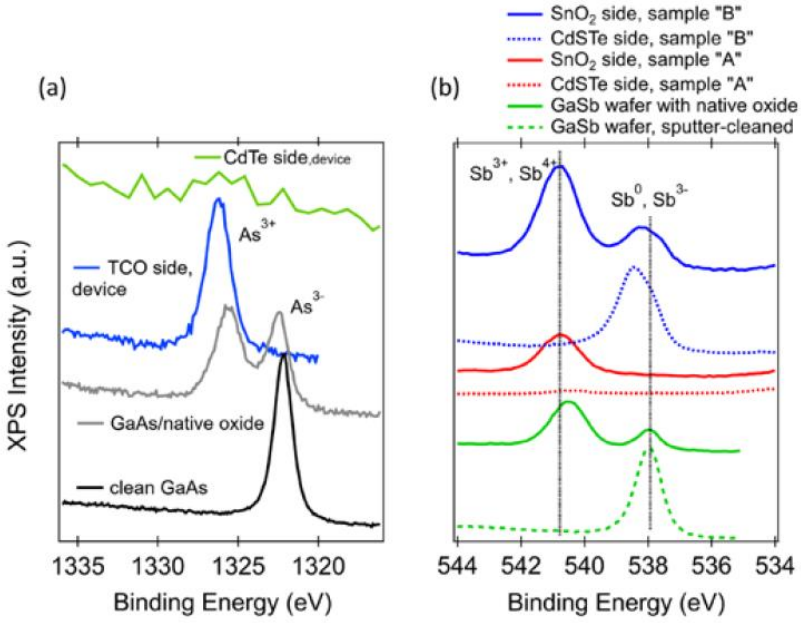

Figure Task 6.4 XPS spectra of the arsenic 2p3/2 region from a cleaved CdTe device, along with spectra from reference materials (a). In panel (b), similar data for antimony doped films.

The incorporation of Group V dopants phosphorus, arsenic, and antimony into CdTe films was studied in Task 6. A number of approaches can incorporate impurity elements into semiconductors to increase the hole density. Silicon technologies have used external diffusion since their inception and, as was stated above, current CdTe solar technology diffuses Cl and Cu into the cell during the $CdCl_2$ and back-contact annealing steps. One advantage with diffusion is that it can be applied after deposition and can thereby be decoupled from the details of the growth processes. Initial efforts examined replacing Cu diffusion with group V dopant diffusion into polycrystalline films. Glass/SnO_2/CdS/CdTe samples were sealed in evacuated ampoules with small amounts of Cd_3P_2, Cd_3As_2 or CdSb, and annealed at temperatures ranging from 550 °C to 700 °C for times ranging from minutes to hours.[5]

To image activation, an electron beam was scanned across a bevelled surface to generate electron–hole pairs with ~100 nm spatial resolution (Fig. Task 6.5a). Cathodoluminescence (CL) spectra were collected at each position, with the sample temperature held at 6 K. Spectra are colour-coded in Fig. to show regions with predominantly excitonic (blue), As_{Te} (green) and deeper (red) emission (Fig. Task 6.5b). CL spectra on as-deposited films indicate that excitonic emission can often be associated with undoped regions. Recent work has demonstrated that P, As and Sb diffuse orders of magnitude more quickly along GBs relative to the grain interior. Figure Task 6.5c illustrates that, after annealing with Cd_3As_2 at 650 °C for 15 min, As is able to penetrate many but not all grains. At the same time, the fast As diffusion along GBs and to the front absorber/buffer interface produces deeper states in these regions that can limit carrier

lifetime and photovoltaic performance. The inhomogeneity and GBs of polycrystalline films shown here complicate uniform dopant incorporation. Furthermore, here, the As diffusion temperature exceeds the softening point of commercial soda-lime glass, and temperatures below the softening point lead to insufficient As incorporation in the grain interior. Phosphorus is a smaller atom that can diffuse throughout the material at lower temperatures by interstitial diffusion; however, an activation step is then more likely to be needed to move interstitial P atoms to Te lattice sites. In addition, smaller atoms substituted on the relatively large Te site have less favorable formation energy and can be more easily displaced by subsequent Cl processes. Consequently, focus has shifted away from diffusion to in situ deposition to overcome hole density limits.

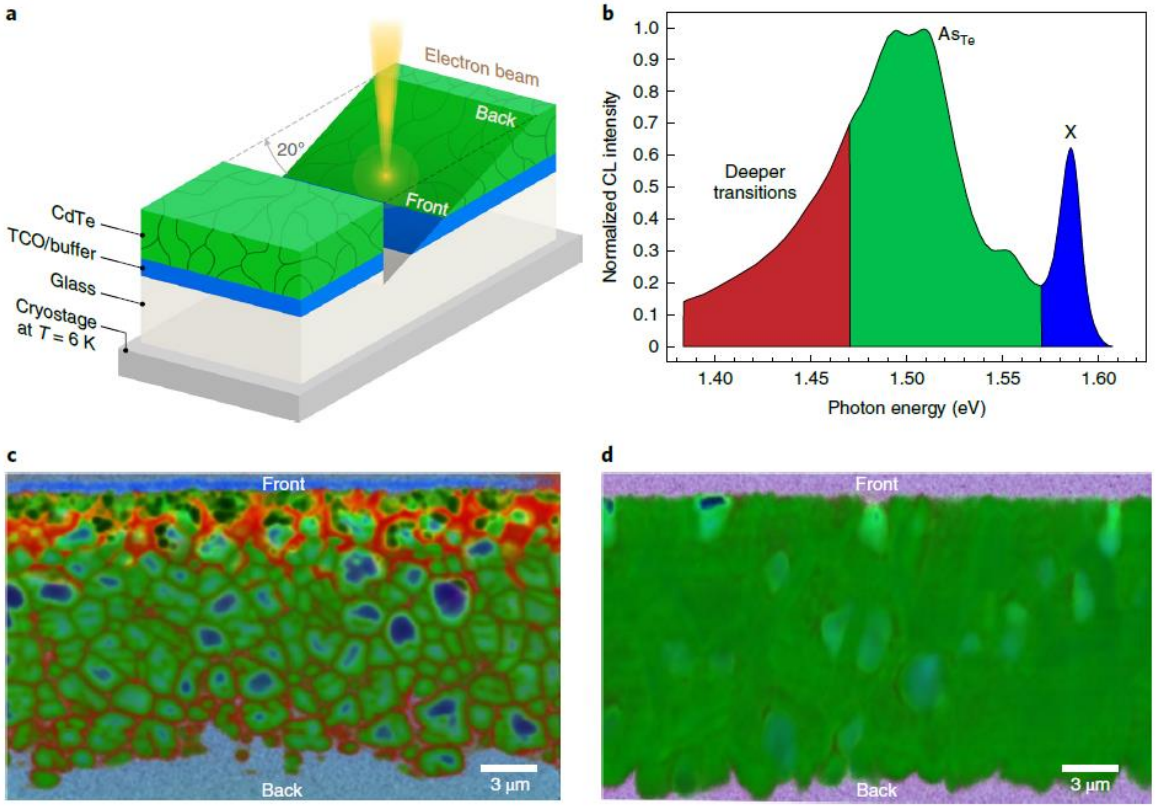

Figure Task 6.5 In (a), a schematic of the CL measurements done on beveled film stacks. In (b), a representative CL spectrum showing excitonic (blue), AsTe (green), and deeper defect (red) emission.

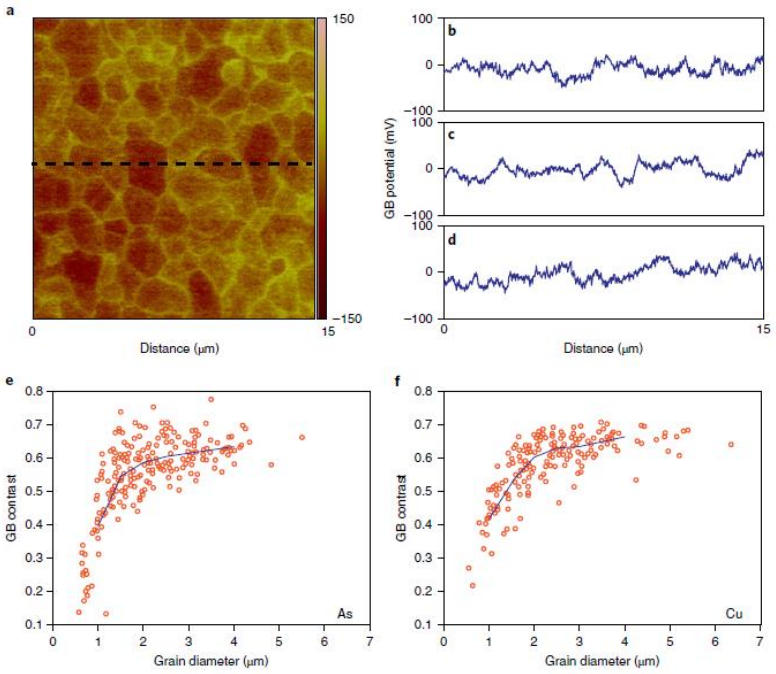

Figure Task 6.6 In upper panels, scanning Kelvin probe microscopy results showing grain-scale potential fluctuations. In lower panels, CL contrast between grain interior and grain boundary as a function of grain diameter.

Another concern addressed within Task 6 is the effect of newer Group V dopants on grain boundary potentials and recombination around grain boundaries. Arsenic that segregates or induces GB defects can form strong electrostatic potentials and attract minority carriers, thereby increasing recombination and/or creating shunt paths. Such effects may be responsible for voltage deficits observed with Group V doped devices. GB potentials were measured on As-doped polycrystalline films using Kelvin probe force microscopy (KPFM) at different film depths (Figure Task 6.6a-b). The results indicate small fluctuations, generally <30 mV, and are insufficient to explain the voltage deficit. Similarly, Figure Task 6.6e and Figure Task 6.6f compare the CL contrast, $((I_{GI} - I_{GB})/I_{GI})$, for hundreds of grains in As-doped and Cu-doped samples. These data, coupled with the lifetime measurements, indicate that enhanced GB recombination is not a likely reason for the observed voltage deficit, an important clue to improving future devices.

Optoelectronic properties of the front interface and of the absorber were examined in this study of state-of-the art Group V doped devices. One experimental approach to assess interface recombination is to extrapolate V_{oc} as a function of temperature to 0 K, where interface recombination and Fermi-level pinning can cause the extraplolated V_{oc} to be less than the bandgap. Figure Task 6.7a shows V_{oc} as a function of temperature for CdTe:As, CdSeTe:As and CdSeTe:Cu. Here, doping with As and not using Se appear to enhance interfacial losses.

Subsequent experiments explored whether the interfacial structural or chemical loss mechanisms could be identified. Aberration-corrected transmission electron microscopy (TEM; not shown) failed to reveal front-extended or structural front-interface defects caused by As or Cu dopants. To examine the interfacial chemistry, samples were planar cleaved at the front interface by carefully attaching epoxy handles and immersing complete devices in liquid nitrogen within a glovebox. This process often produces atomically smooth planar cleaves with minimized

exposure of the interface to contamination or oxidation. X-ray photoemission spectroscopy (XPS) was then applied to measure the nanometer-scale interfacial chemistry for As-doped samples. Figure Task 6.7b shows spectra of the As $2p_{3/2}$ region taken on the TCO side of cleaved devices, which indicate that As in some conditions can segregate as As^{3+} at the SnO_2 interface. To be detected by XPS, the As concentration must be $>1 \times 10^{20}$ cm^{-3}. Detailed analysis and a lack of signal on the absorber side of the cleaved surface indicate that the As is probably in monolayer form. By varying the incorporation level, annealing conditions and interface chemistry, the interface accumulation can be modulated, as shown by the blue trace in Figure Task 6.7b. At this time, we cannot state with certainty that high interfacial As levels cause increased recombination or lower V_{oc}. However, the results do indicate that doping can significantly affect the interfacial chemistry in ways not anticipated.

Potential fluctuations introduced by electrostatic charge from compensating donors and acceptors can also cause voltage loss and be evaluated from spectral analysis of luminescence spectra. In planar cleaved samples, the full-width at half-maximum (FWHM) in photoluminescence and CL spectra (Figure Task 6.7c) increases with As relative to Cu at the front interface. CL microscopy reveals that the FWHM differences occur within individual CdSeTe grain interiors. Both photoluminescence and CL indicate that potential fluctuations can range from 50 meV to more than 100 meV, which can account for a substantial fraction of the observed voltage loss. To confirm that this effect is due to As doping rather than Se alloying with a different experimental method, absorption was measured on CdTe films (Figure Task 6.7d). Consistent with the luminescence broadening, below-bandgap absorption increases with increasing As levels.

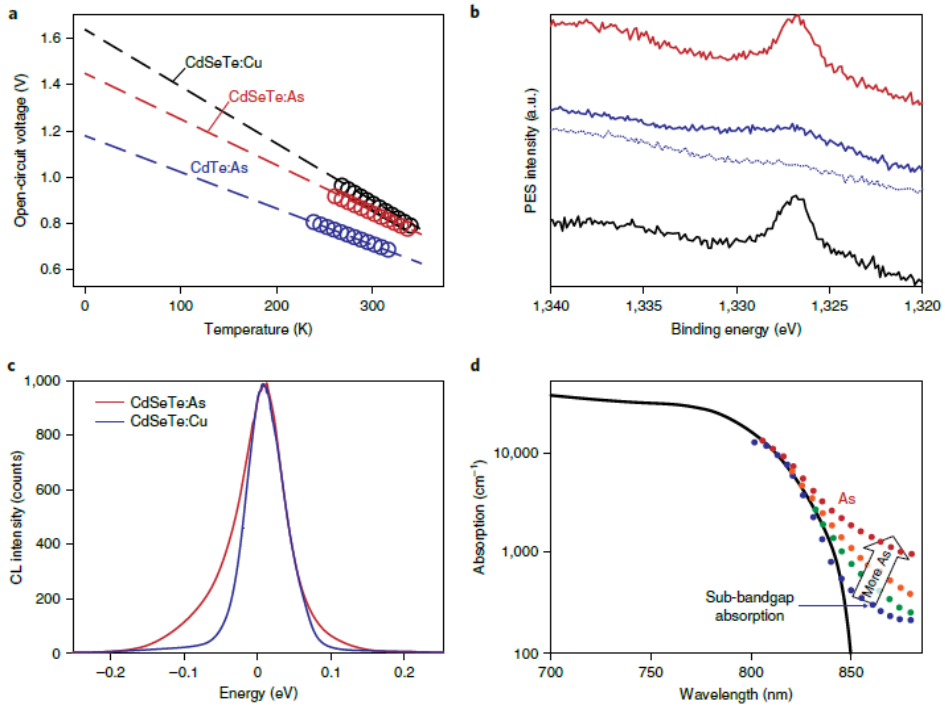

Figure Task 6.7 In (a), Voc versus T data comparing Se alloying and doping conditions. In (b) XPS data of the As 2p3/2 region indicating that arsenic segregations can be alleviated with processing. Band tails due to arsenic were found using CL spectra (c) and optical absorption measurements (d)

References:

[1] D. Kuciauskas, P. Dippo, A. Kanevce, Z. Zhao, L. Cheng, A. Los, M. Gloeckler, and W.K. Metzger, Appl. Phys. Lett. **107**, 243906 (2015).

[2] D. Kuciauskas, P. Dippo, Z. Zhao, L. Cheng, A. Kanevce, W.K. Metzger, and M. Gloeckler, IEEE J. Photovoltaics **6**, 313 (2016).

[3] J. Moseley, S. Grover, D. Lu, G. Xiong, H.L. Guthrey, M.M. Al-Jassim, and W.K. Metzger, Journal of Applied Physics **128**, (2020).

[4] C.L. Perkins, B. McCandless, D.L. McGott, M.O. Reese, and W. Metzger, in *2019 IEEE 46th Photovoltaic Specialists Conference (PVSC)* (2019), pp. 0169–0172.

[5] W.K. Metzger, S. Grover, D. Lu, E. Colegrove, J. Moseley, C.L. Perkins, X. Li, R. Mallick, W. Zhang, R. Malik, J. Kephart, C.-S. Jiang, D. Kuciauskas, D.S. Albin, M.M. Al-Jassim, G. Xiong, and M. Gloeckler, Nat Energy 1 (2019).

Subject Inventions Listing: None.

ROI #: None.